International Journal of Advanced Engineering and Technology Research
ISSN: 3106-8677 (Print), ISSN: 3106-8685 (Online) | Vol. 2, No. 2, 2026

Study on the Enhanced-Gravity Separation Characteristics of Copper Ore in a Spiral Trapezoidal Pipe

Guojun Song, Zhongbin Liu

College of mechanical engineering, Sichuan University of science & engineering, Yibin 643000, China

Abstract: To address the difficulty in separating low-grade, fine-grained and severely slimed copper ores, this study combines the advantages of enhanced-gravity separation technology and continuous separation in a spiral flow channel, and proposes an enhanced-gravity separation method using a spiral trapezoidal pipe. In this method, an enrichment section and a secondary sand-splitting section are arranged successively along the flow direction, forming a gradient separation structure. In the enrichment section, the centrifugal force field generated by the spiral flow channel promotes the preliminary enrichment of Cu particles. In the secondary sand-splitting section, local recirculation vortices and reverse radial flow are induced by abrupt cross-sectional expansion, thereby strengthening the separation of light and heavy particles. Fluent was used to numerically simulate the flow-field distribution, recirculation vortex evolution, particle distribution characteristics, and the influence of structural parameters on the separation performance of the spiral trapezoidal pipe under enhanced-gravity separation. The results show that the stable radial pressure gradient and relatively high tangential velocity in the enrichment section are conducive to the migration of Cu particles toward the outer enrichment wall. In the secondary sand-splitting section, the recirculation vortex first strengthens, then weakens, subsequently decays slowly, and finally disappears rapidly along the flow direction. The recirculation vortex in the front part strips SiO_2 particles from the surface layer of the particle bed, while the negative radial-velocity region at the bottom of the middle and rear parts further promotes the lateral entrainment of SiO_2 particles from the outer enriched bed toward the inner mainstream region. The particle volume fraction distribution indicates that Cu particles are mainly and stably enriched in the outer bottom region, whereas SiO_2 particles gradually migrate toward the newly formed cavity and the tailings side. The structural parameter analysis shows that when the spiral diameter is 260 mm, the pitch is 50 mm, and the boss width of the secondary sand-splitting section is 4 mm, the spiral trapezoidal pipe exhibits better separation performance, with a Cu recovery of 72.35% and an enrichment ratio of 10.51. The results can provide a reference for the enhanced separation of low-grade, fine-grained complex copper ores and the structural design of novel enhanced-gravity separation equipment.

Keywords: Copper ore, enhanced-gravity separation, gradient separation, recirculation vortex.

1. Introduction

Copper, as an important non-ferrous metal resource, is widely used in electrical engineering, machinery manufacturing, new energy, transportation and other fields. In recent years, with the rapid development of industries such as new energy vehicles, wind power, photovoltaics and energy storage, the demand for copper resources has continued to increase [1, 2]. However, copper resources in China are relatively insufficient, and copper ores generally exhibit characteristics such as low grade, fine dissemination size, severe sliming and high clay mineral content [3], which makes the efficient separation and recovery of copper ores increasingly difficult. In particular, with the gradual decrease in easily beneficiated copper sulfide resources, the proportion of complex and refractory resources such as copper oxide ores and mixed copper ores has increased [4], placing higher requirements on separation technologies.

At present, copper ore recovery still mainly relies on flotation [3, 4]. However, when treating complex copper ores with low grade, fine particle size, high oxidation rate and severe sliming, the flotation performance is often limited. On the one hand, fine copper particles are small in size and light in mass, resulting in a low probability of collision and attachment with bubbles, which easily causes the loss of valuable minerals. Meanwhile, fine slimes can cover mineral surfaces, increase slurry viscosity and induce non-selective adsorption of reagents, thereby reducing separation selectivity and increasing reagent consumption [5-7]. On the other hand, for poorly floatable copper oxide ores and mixed ores, flotation usually requires sulfidization pretreatment or collectors with relatively weak selectivity [3, 4], which may lead to a longer flowsheet, higher cost and increased environmental risks. Therefore, developing an efficient, low-consumption and environmentally friendly separation method suitable for fine-grained complex copper ores is of great significance.

Gravity separation has the advantages of a simple process, low operating cost and environmental friendliness [8]. Among gravity separation equipment, spiral separators have been widely used in mineral separation because of their simple structure, large processing capacity and strong continuous operation capability. However, conventional spiral separators mainly rely on the gravity field and limited centrifugal effect, and their separation force field is relatively weak. When treating low-grade, fine-grained and severely slimed minerals, problems such as insufficient particle stratification, unclear boundaries of the enrichment zone and inadequate selective separation ability are likely to occur [9]. In contrast, enhanced-gravity separation can amplify the force difference between light and heavy particles by strengthening the centrifugal force field, which is beneficial for improving the stratification and enrichment of fine-grained minerals [10]. Nevertheless, existing centrifugal separation equipment

generally has shortcomings such as complex structure, high energy consumption, high operation and maintenance requirements, and difficulty in simultaneously achieving continuous and stable discharge.

Based on this, this study takes a low-grade copper ore from Tibet with fine particle size, high oxidation rate and severe sliming as the research object, and proposes an enhanced-gravity spiral trapezoidal pipe separation model. On the basis of retaining the continuous separation characteristics of the spiral flow channel, this model introduces an intensified centrifugal force field and promotes the preliminary enrichment of copper particles and the enhanced separation of light and heavy particles through the structural coordination between the enrichment section and the secondary sand-splitting section. This study focuses on analyzing the internal flow-field evolution characteristics of the model and their influence on particle migration and separation, and reveals the interaction mechanism between preliminary stratification in the enrichment section and enhanced separation in the secondary sand-splitting section. The results are expected to provide a reference for the efficient separation of fine-grained complex copper ores and the design of novel enhanced-gravity separation equipment.

2. Separation Mechanism of the Spiral Trapezoidal Pipe

2.1. Basic Structure of the Spiral Trapezoidal Pipe

Figure 1 shows the structural schematic of the spiral trapezoidal pipe. The main body of the model is a fixed three-and-a-half-turn spiral flow channel. The inlet end serves as the slurry inlet, while a thin-plate splitter is arranged at the end of the flow channel to divide the outlet cross-section into the outer concentrate outlet and the inner tailings outlet, thereby realizing the separated collection of minerals. Along the flow direction, the spiral trapezoidal pipe is divided into an enrichment section and a secondary sand-splitting section, among which the first three turns serve as the enrichment section and the last half turn serves as the secondary sand-splitting section.

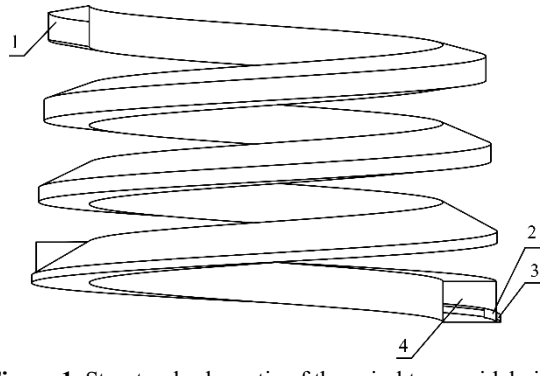

Figure 1. Structural schematic of the spiral trapezoidal pipe

Notes: 1-Slurry inlet; 2-Thin-plate splitter; 3-Concentrate outlet; 4-Tailings outlet.

As shown in Figure 2, the cross-sectional area along the enrichment section remains basically constant, while the cross-sectional shape gradually transitions from an isosceles trapezoid at the inlet to a narrow and tall right trapezoid. Specifically, the length of the inner wall near the central axis remains unchanged, whereas the length of the enrichment wall far from the central axis gradually decreases and shifts downward along the axial direction. Meanwhile, the radial spacing between the two side walls gradually increases, so that the cross-sectional flow area remains essentially unchanged during the geometric transition.

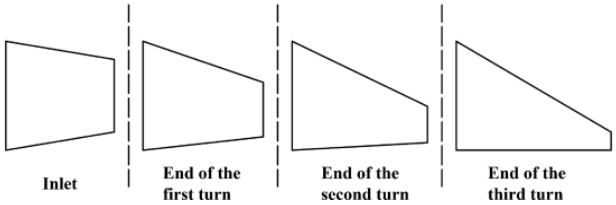

Figure 2. Schematic diagram of cross-sectional variation in the enrichment section

As shown in Figure 3, the main geometric difference between the secondary sand-splitting section and the enrichment section lies in the local abrupt expansion of the upper space of the flow channel, which forms an additional cavity connected to the original channel.

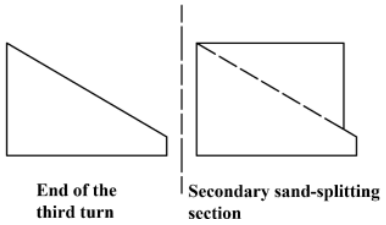

Figure 3. Schematic diagram of cross-sectional abrupt expansion in the secondary sand-splitting section

2.2. Separation Principle of the Spiral Trapezoidal Pipe

The separation process in the spiral trapezoidal pipe is as follows. The slurry enters the spiral flow channel tangentially from the slurry inlet under a certain pressure, forming a high-speed rotating spiral flow field. Under the combined effects of centrifugal force, buoyancy, gravity and fluid drag, mineral particles begin to stratify according to their density differences. Heavy mineral particles are subjected to greater centrifugal acceleration, rapidly migrate toward the outer enrichment wall region, and settle on the enrichment wall surface. In contrast, most light mineral particles remain on the inner side or in the surface layer of the particle bed. As the concentration of the outer particle bed increases, the contracted outer-wall structure of the trapezoidal cross-section in the enrichment section significantly increases the velocity gradient and shear stress near the wall. This effectively disrupts the dense packing of particles under the strong centrifugal force field, keeps the particle bed in a loose and fluidized state, and facilitates the continuous interstitial percolation of heavy particles toward the outer wall surface.

As shown in Figure 4, when the particle bed enters the secondary sand-splitting section from the enrichment section, the average velocity of the mainstream decreases and the static pressure increases because of the sudden enlargement of the channel cross-sectional area, resulting in an obvious adverse pressure gradient along the flow direction. Under the action of this adverse pressure gradient, the boundary-layer fluid near the upper region of the enrichment section lacks sufficient momentum to maintain wall-attached flow. As the wall shear stress approaches zero, flow separation occurs in the slurry, and a relatively stable recirculation vortex region forms in the abruptly expanded cavity. A free shear layer is formed between the separated recirculation region and the high-speed mainstream below. This shear layer continuously

undergoes entrainment and momentum exchange with both the high-speed mainstream below and the recirculation region. As it moves downstream, it gradually approaches the sloped wall under the combined effects of centrifugal force and geometric guidance, and reattaches to the wall at a certain position. At this point, the wall shear stress changes from negative to positive, the shear layer is compressed into a thin wall-attached layer, and two weak jets develop upstream of the reattachment point. One weak jet moves upward along the sloped wall, forming a wall-attached upward weak jet. This jet imposes strong shear on the light particles at the surface of the particle bed, causing gangue mineral particles to be stripped from the bed surface and entrained into the newly formed upper cavity. The other weak jet extends downward along the sloped wall, forming a wall-attached downward weak jet. This jet produces a shear distribution that gradually weakens in the particle bed, continuously refreshes the boundary layer on the bed surface, weakens the bonding effect of fine slimes, and inhibits the re-compaction of the particle bed.

Through the abrupt expansion structure of the flow-channel cross-section, the secondary sand-splitting section induces local flow-field reconstruction. Without changing the geometric morphology of the outer particle enrichment cross-section, it realizes washing of the particle-bed surface. Low-density gangue mineral particles are entrained by the upward weak jet into the newly formed cavity and discharged with the tailings, whereas heavy mineral particles, owing to their greater inertia and more stable attachment, overcome the influence of the downward weak jet and remain stably enriched in the outer sloped region, thereby improving the concentrate grade.

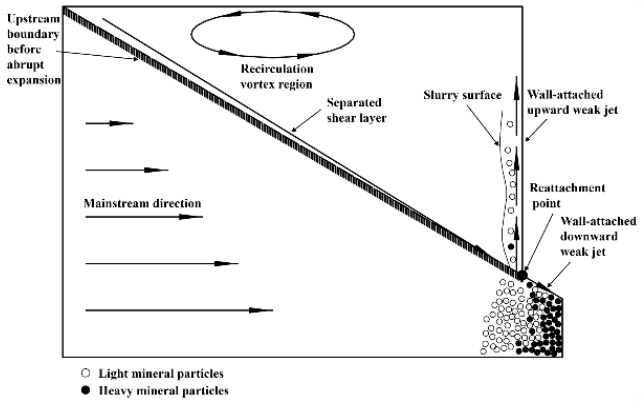

Figure 4. Separation principle diagram of the secondary sand-splitting section

2.3. Analysis of Particle Forces and Motion Laws in the Separation Flow Field

Particles with different densities are subjected to different effects of centrifugal force, fluid drag and other forces, resulting in significant differences in their motion trajectories and velocity distributions. In the centrifugal separation flow field, solid particles are acted upon by centrifugal force, buoyancy, fluid viscous drag, gravity and other forces, as shown in Figure 5.

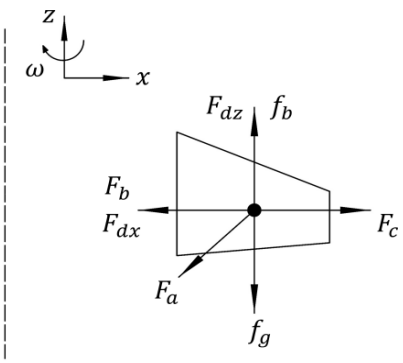

Figure 5. Force analysis of particles

During centrifugal separation, the separation effect mainly occurs in the radial motion process. At this stage, the forces acting on a spherical particle in the radial direction include:

Centrifugal force F_c:

$$F_c = \frac{\pi}{6} d_s^{\,3} \rho_s r \omega^2 \tag{1}$$

Buoyancy in the centrifugal force field F_b:

$$F_b = \frac{\pi}{6} d_s^{\,3} \rho_f r \omega^2 \tag{2}$$

Drag force F_d:

$$F_{\mathrm{d}} = \frac{\pi d_s^2}{4} \frac{C_D}{2} \rho_f \left(u_s - u_f\right)^2 \tag{3}$$

Added mass force F_a:

$$F_a = \frac{\pi d_s^3 \rho_f}{12} \left(\frac{\mathrm{d}u_s}{\mathrm{d}t} - \frac{\mathrm{d}u_f}{\mathrm{d}t} \right) \tag{4}$$

Where d_s is the mineral particle diameter, m; ρ_s and ρ_f are the densities of the mineral particle and the fluid, respectively, kg/m³; r is the instantaneous radial position of the mineral particle from the central axis of the spiral trapezoidal pipe, m; ω is the centrifugal angular velocity, rad/s; $u_s$and $u_f$are the velocities of the mineral particle and the fluid, respectively, m/s.

According to Newton's second law, the radial equation of motion of a particle can be expressed as:

$$F_{\mathrm{c}} - F_{\mathrm{dx}} - F_{\mathrm{b}} - F_{\mathrm{ax}} = m(\mathrm{d}u_{\mathrm{px}} / \mathrm{d}t) \tag{5}$$

By substituting Eqs. (1), (2), (3) and (4), the dynamic equation of the particle in the radial direction can be obtained as:

$$\begin{aligned} &\left(\frac{\rho_{\mathrm{s}}}{\rho_f} + \frac{1}{2} \right) \frac{du_{\mathrm{sx}}}{dt} = \left(\frac{\rho_{\mathrm{s}}}{\rho_f} - 1 \right) r\omega^2 \\ &- \frac{3C_{\mathrm{D}}}{4d_{\mathrm{s}}} \left(u_{\mathrm{sx}} - u_{fx}\right)^2 + \frac{1}{2} \frac{du_{fx}}{dt} \end{aligned} \tag{6}$$

Equation (6) is the basic equation of particle motion. It can be seen that the particle motion behavior is related to the centrifugal acceleration $(r\omega^2)$, fluid velocity $\left(u_{fx}\right)$, and fluid acceleration $\left(du_{fx}/dt\right)$. The first term is the centrifugal acceleration term, indicating that a greater density difference

between the particles to be separated makes particle separation easier. The second term is the drag acceleration term caused by the relative motion between the particle and the fluid medium. It is related to particle density, particle size and particle shape, and is proportional to the square of the relative velocity between the particle and the fluid. The third term is the inertial acceleration term induced by the acceleration of the fluid medium. When the medium density is constant, this term is only related to particle density and is beneficial for density-based particle stratification.

3. Numerical Simulation of the Separation Model

3.1. Establishment of the Simulation Model

To further investigate the motion characteristics of particles in the enhanced-gravity spiral trapezoidal pipe, SolidWorks three-dimensional modeling software was used to establish the fluid domain of the spiral trapezoidal pipe, which was then imported into ANSYS Workbench. The fluid domain was subsequently defined with boundary conditions, including the feed inlet inlet, concentrate outlet outlet1, tailings outlet outlet 2, and wall surface wall, as shown in Figure 6. The main structural parameters of the model are listed in Table 1.

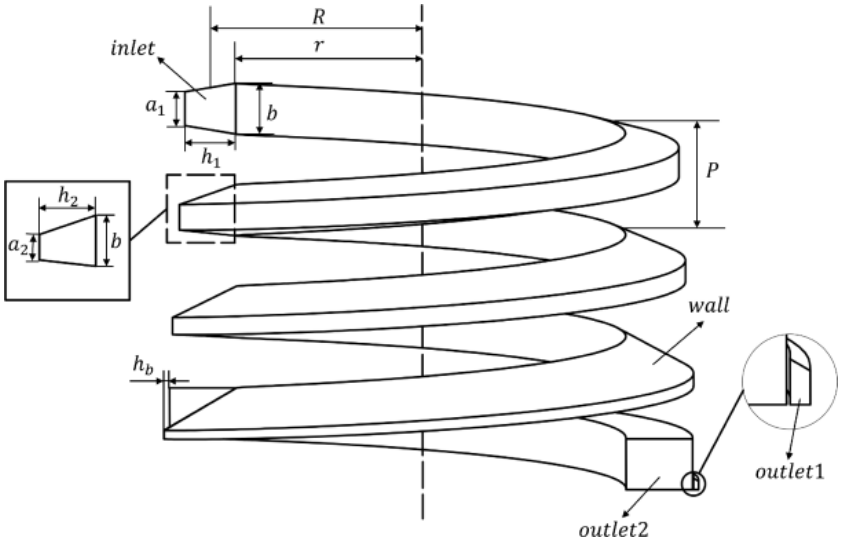

Figure 6. Structure of the fluid-domain model

Table 1. Main structural parameters of the model

Structure	Parameter
Equivalent spiral radius R, pitch P	150 mm, 60 mm
Inner radius r, number of turns N	135 mm, 3.4
Inner wall size b	30 mm
Outer wall sizes a_1, a_2, a_3, a_4	20 mm, 15 mm, 10 mm, 5 mm
Horizontal spacing between the inner and outer walls h_1, h_2, h_3, h_4	30 mm, 33.33 mm, 37.5 mm, 42.86 mm
Boss width of the secondary sand-splitting section h_b	3 mm

3.2. Material Parameters

In this study, a copper ore from Tibet was selected as the research object. The Cu grade of the ore is 0.5%, and the SiO_2 content is as high as 69.2%, indicating that it is a low-grade, high-silica refractory copper oxide ore. The ore has a relatively high degree of sliming, and the copper minerals are finely disseminated. The copper mainly occurs in the form of copper sulfides and partially oxidized copper minerals. The copper sulfide minerals mainly include bornite, chalcocite, covellite and copper-blue sulfur-bearing minerals, while the oxidized copper minerals mainly include malachite, azurite and chrysocolla. The main chemical compositions are shown in Table 2.

Table 2. Main chemical compositions of a copper ore from Tibet / %

Component	Cu	S	Mo	Pb	Zn	Fe	CaO	MgO	Al_2O_3	SiO_2	Au*
Content	0.5	1.45	0.011	0.01	0.01	1.72	1.68	0.82	15.03	69.12	0.02

3.3. Simulation Settings and Boundary Conditions

To simplify the calculation and solution process, the mineral components were simplified during the simulation. Cu particles and SiO_2 particles were used to represent heavy minerals and light minerals, respectively, with densities of 6300 kg/m³ and 2650 kg/m³. The particle diameter was set to 0.074 mm, and water was used as the separation medium. According to the Cu grade of the raw ore, the solid–liquid ratio was set as 80% water, 19.9% SiO_2 and 0.1% Cu.

To investigate the multiphase flow and particle separation characteristics in the enhanced-gravity spiral trapezoidal pipe, considering that the fluid medium is incompressible, the Pressure-Based solver was adopted. The calculation was performed using a Transient solver, and the velocity

formulation was set to Absolute. The multiphase flow was modeled using the Eulerian model, and the interphase drag between the solid and liquid phases was treated using the Gidaspow model. The RNG k-ε model was selected as the turbulence model, and the near-wall region was treated using enhanced wall functions. The boundary conditions were set as follows: the inlet was defined as a velocity inlet with an inlet velocity of 8 m/s, and the volume fractions of each phase were specified; the outlets were defined as pressure outlets with the pressure set to one standard atmosphere; all walls were set as no-slip stationary walls.

4. Results and Analysis

4.1. Flow-Field Analysis of the Enrichment Section

To analyze the internal flow-field distribution in the enrichment section, a horizontal reference line was selected every 180° along the spiral direction. The line extended from the midpoint of the outer enrichment wall to the inner wall, and the pressure, radial velocity and tangential velocity distribution curves were extracted, as shown in Figure 7.

As shown in Figure 7(a), the pressure in the enrichment section gradually increases in the radial direction from the inner wall to the outer enrichment wall, forming a relatively stable radial pressure gradient. When the ore slurry flows through the spiral channel, the outer region is more strongly affected by centrifugal action, making high-density Cu particles more likely to migrate toward the outer enrichment wall. As the spiral angle increases, the pressure of each cross-section generally shows a decreasing trend, which is mainly related to friction loss along the flow path, viscous dissipation and fluid energy loss. A local negative-pressure region appears at the 360° cross-section of the third turn. This position is related to the cross-sectional abrupt-expansion structure of the secondary sand-splitting section. After the fluid enters the abrupt-expansion region, flow expansion and recirculation reconstruction occur, resulting in a decrease in local static pressure.

Radial velocity is an important factor affecting the lateral migration and stratified enrichment of particles. As shown in Figure 7(b), the radial velocity in the enrichment section first increases and then decreases, reaching a relatively high value in the middle region of the cross-section. This region is the main area for lateral particle migration and is favorable for the movement of Cu particles toward the outer enrichment wall. The radial velocity distributions at different spiral angles are basically similar, indicating that the radial migration effect in the enrichment section is relatively stable and helps maintain the stratified state of light and heavy particles. At the 360° cross-section of the third turn, the radial velocity in the abrupt-expansion region increases significantly, mainly because the abrupt-expansion structure enhances the local radial transport capacity, providing flow conditions for the subsequent re-separation of particles in the secondary sand-splitting section.

Tangential velocity is the basis for forming the centrifugal force field, and its magnitude directly affects the centrifugal action experienced by particles. As shown in Figure 7(c), the tangential velocity in the enrichment section remains at a relatively high level overall, indicating that a stable rotating flow is formed in the spiral channel. The tangential velocity increases rapidly in the radial direction from the inner wall to the outer side and maintains a relatively high value from the middle to the outer region of the cross-section, providing continuous centrifugal action for the migration of particles toward the outer enrichment wall. The tangential velocity decreases near the outer wall, mainly because the wall viscous resistance reduces the flow velocity in the near-wall region. Overall, the enrichment section can maintain a stable radial pressure gradient, radial migration velocity and relatively high tangential velocity, providing fundamental flow-field conditions for the continuous migration of high-density Cu particles toward the outer enrichment wall and for subsequent secondary sand-splitting.

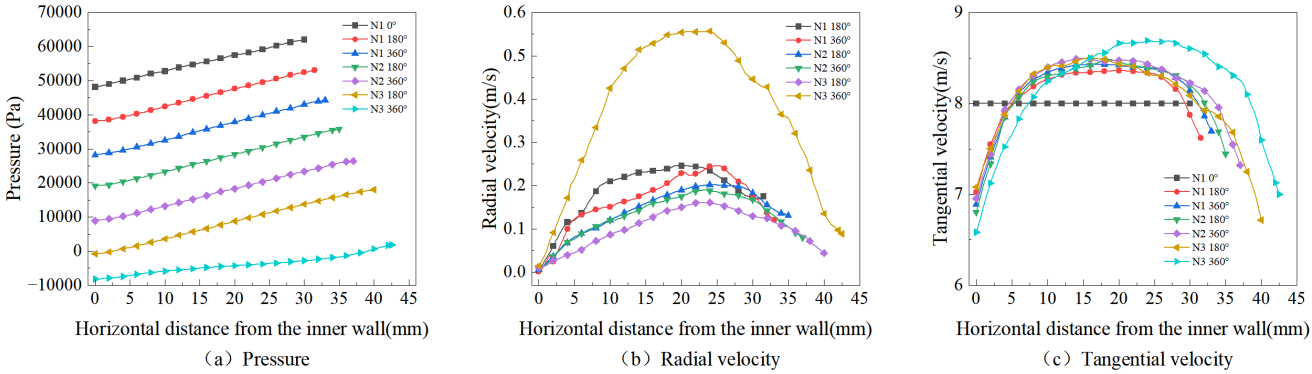

（a）Pressure　（b）Radial velocity　（c）Tangential velocity

Figure 7. Distribution curves of pressure, radial velocity and tangential velocity in the enrichment section

4.2. Flow-Field and Recirculation Vortex Analysis of the Secondary Sand-Splitting Section

To analyze the local flow-field evolution in the secondary sand-splitting section, cross-sections at different spiral angles in the fourth turn were selected. The axial velocity, recirculation vortex streamlines, recirculation vortex intensity and radial velocity distribution were analyzed, as shown in Figs. 8~10. Here, the I side refers to the inner wall close to the central axis, while the K side refers to the outer wall far from the central axis. The axial velocity takes the vertically upward direction as positive, and the radial velocity takes the direction from the central axis toward the outer wall as positive.

As shown in Figure8, localized upward flow opposite to the mainstream direction appears in the secondary sand-splitting section, forming an obvious closed recirculation vortex structure. After the slurry enters the secondary sand-splitting section from the enrichment section, the average velocity of the mainstream decreases due to the abrupt expansion of the cross-section. Under the action of a local adverse pressure gradient, flow separation occurs, and a separated recirculation region forms inside the abruptly expanded cavity. In the

5°~65° cross-sections of the fourth turn, the flow field is mainly characterized by a counterclockwise single-vortex structure. The recirculation vortex first appears in the upper part of the abruptly expanded cavity and gradually migrates toward the inner side and middle region as the flow develops. At this stage, the upward jet and the recirculation vortex mainly act on the surface layer of the outer enriched bed, exerting shear and entrainment on SiO_2 particles with lower density and weaker inertia, making them more likely to detach from the bed surface or interparticle pores and enter the upper newly formed cavity. In contrast, Cu particles, owing to their higher density and greater inertia, settle more stably and mainly remain in the outer boss region. In the 75°~100° cross-sections of the fourth turn, the flow field gradually evolves from a single counterclockwise vortex into a double-vortex coexisting structure with opposite rotational directions. Specifically, the upper clockwise vortex gradually strengthens, whereas the lower counterclockwise vortex gradually weakens. After the 100° cross-section of the fourth turn, the recirculation vortex gradually weakens. By the 135° cross-section of the fourth turn, the closed recirculation vortex structure has basically disappeared, and the flow field at the rear part of the secondary sand-splitting section gradually shifts to a relatively stable downward transport state.

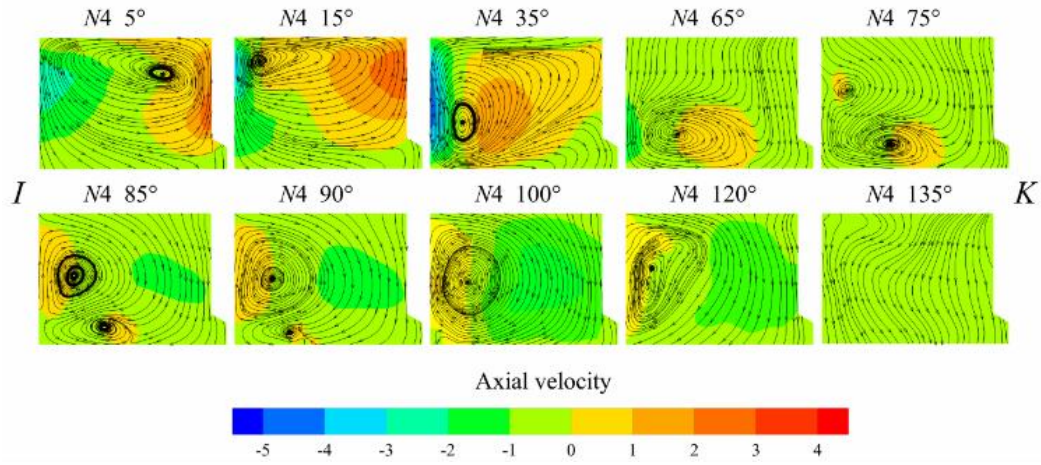

Figure 8. Axial velocity distribution and streamlines of recirculation vortices

To analyze the variation in recirculation intensity within the flow field of the secondary sand-splitting section, the dimensionless number J_z was introduced. The recirculation vortex can be characterized by the area-averaged absolute value of the vorticity on the flow-direction cross-section, as shown in Eq. (7) [11, 12]:

$$J_z = \frac{1}{A}\iint_A |\omega_z| \, \mathrm{d}A \tag{7}$$

where A is the cross-sectional area, m²; and ω_z is the average vorticity normal to the cross-section, s⁻¹.

In Tecplot, one cross-section was extracted every 5° along the secondary sand-splitting section, and the absolute value of the vorticity normal to each cross-section was area-averaged to obtain the variation curve of recirculation vortex intensity along the flow path, as shown in Figure 9. It can be seen that the recirculation vortex intensity in the secondary sand-splitting section first increases, then decreases, subsequently decays slowly, and finally disappears rapidly along the flow direction. Within the range of 5°~20° in the fourth turn, the separated recirculation induced by the abrupt expansion is relatively strong, and the recirculation vortex intensity increases rapidly to its peak, which is favorable for stripping SiO_2 particles from the surface layer of the particle bed. Within the range of 20°~75° in the fourth turn, the recirculation vortex migrates and expands downstream, and its intensity decreases significantly. Within the range of 75°~100° in the fourth turn, the coexistence of double vortices keeps the recirculation vortex intensity at a moderate level and allows it to decay slowly. After 100° in the fourth turn, the recirculation vortex intensity decreases rapidly until the closed recirculation structure at the rear of the secondary sand-splitting section gradually disappears.

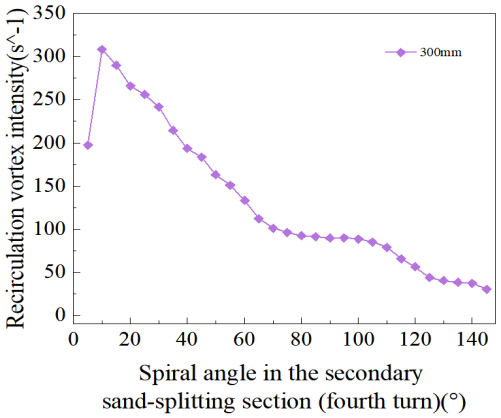

Figure 9. Variation curve of recirculation vortex intensity along the flow path

As shown in Figure 10, with the streamwise evolution of the recirculation vortex, a relatively obvious negative radial-velocity region appears at the bottom of the middle and rear parts of the secondary sand-splitting section. This is particularly evident near the 65°~120° cross-sections of the fourth turn, where the near-bed fluid moves from the outer enrichment wall toward the central axis. At this stage, the radial velocity at the bottom of the particle bed is reversed. Owing to their lower density and weaker inertia, the light particles are more loosely associated with the particle bed and are more easily transported by the reverse radial flow from the outer enriched bed toward the inner mainstream region. In contrast, Cu particles have higher density and greater inertia, and their deposition is relatively stable. Therefore, they can overcome the influence of the local reverse radial flow and mainly remain in the outer boss region. Within the 120°~135° cross-sections of the fourth turn, the bottom negative radial-velocity region gradually shrinks, and the lateral entrainment effect weakens. As a result, the rear part of the secondary

sand-splitting section gradually enters the flow-splitting stage of light and heavy particles.

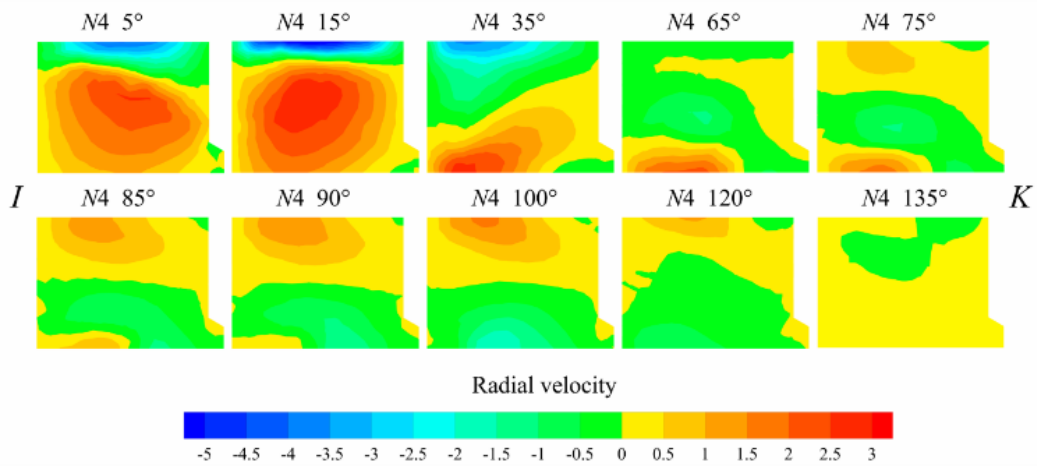

Figure 10. Radial velocity contour

4.3. Distribution Characteristics of Mineral Particles

To analyze the distribution patterns of light and heavy particles in the enrichment section and the secondary sand-splitting section, the volume fraction contours of Cu particles and SiO_2 particles at different spiral-angle cross-sections were extracted, as shown in Figure 11. As shown in Figure 11(a), under the action of centrifugal force, Cu particles gradually migrate toward the outer enrichment wall in the enrichment section as the spiral angle increases. The high-volume-fraction region gradually contracts from the interior of the cross-section toward the outer bottom region, and a relatively obvious heavy-particle enriched bed is formed near the 360° cross-section of the third turn. After entering the secondary sand-splitting section, the high-volume-fraction region of Cu particles is mainly concentrated in the outer bottom boss region. Although local recirculation and reverse radial flow cause certain disturbances to the outer particle bed, Cu particles, owing to their higher density and greater inertia, still remain stably in the outer bottom enrichment region overall.

As shown in Figure 11(b), SiO_2 particles also show a tendency to migrate outward in the enrichment section. However, their distribution range is wider, and their degree of concentration on the outer side is weaker than that of Cu particles. Some light particles are still distributed in the surface layer of the particle bed and inside the cross-section. After entering the secondary sand-splitting section, the distribution of SiO_2 particles in the newly formed cavity and the middle-to-upper region gradually increases, while the enrichment degree near the outer boss decreases. The recirculation vortex and upward jet in the front part promote the detachment of SiO_2 particles in the surface layer of the particle bed from the outer enrichment region. The reverse radial flow in the middle and rear parts further drives SiO_2 particles to migrate toward the inner mainstream region and the tailings channel. Consequently, Cu particles are stably enriched in the outer bottom region, whereas SiO_2 particles gradually detach from the outer particle bed in the secondary sand-splitting section and are carried away.

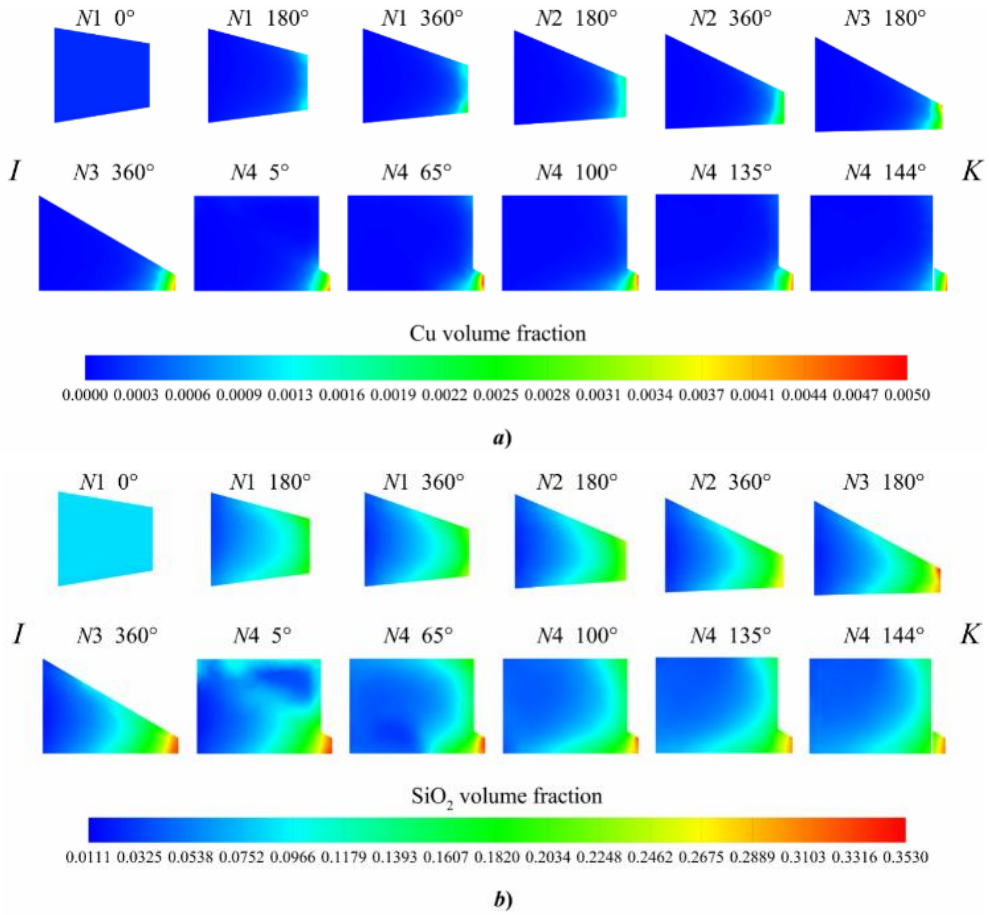

Figure 11. Volume fraction contours of light and heavy particles

4.4. Influence of Structural Parameters on Separation

4.4.1. Influence of Spiral Diameter on Separation

Spiral diameters of 220, 240, 260, 280, 300 and 320 mm were set to compare and analyze the recirculation vortex intensity in the secondary sand-splitting section, Cu recovery and enrichment ratio under different spiral diameters. The spiral diameter changes the curvature of the flow channel and the spiral-flow radius, thereby affecting the radial migration ability of particles in the enrichment section, the axial transport characteristics, and the recirculation-based re-separation effect in the secondary sand-splitting section. As the spiral diameter increases, the curvature of the flow channel decreases, and the radial velocity and axial velocity in the enrichment section generally decrease. As a result, the ability of particles to migrate toward the outer enrichment wall is weakened. As shown in Figure 12, with increasing spiral diameter, the recirculation vortex intensity in the secondary sand-splitting section decreases overall, indicating a reduction in the local flow-field reconstruction ability. Under smaller spiral diameters, the recirculation vortex intensity is relatively high, which is beneficial for stripping and entraining SiO_2 particles from the surface layer of the particle bed. However, excessively strong recirculation disturbance may also affect the stability of the outer enriched bed, causing partial loss of enriched Cu particles. Under larger spiral diameters, the recirculation vortex intensity decreases, resulting in insufficient secondary sand-splitting action. Meanwhile, the radial migration ability in the enrichment section is weakened, which is unfavorable for the sufficient migration of Cu particles toward the outer enrichment wall.

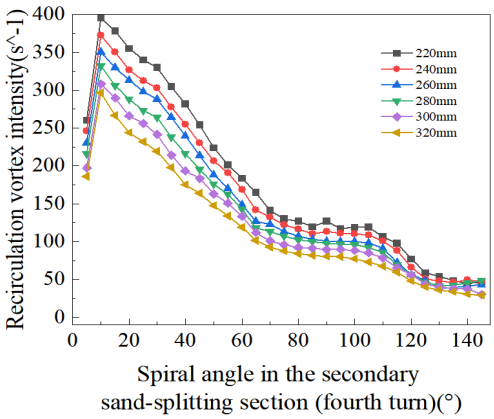

Figure 12. Influence of spiral diameter on recirculation vortex intensity

As shown in Figure 13, the Cu recovery first increases and then decreases with the change in spiral diameter, whereas the enrichment ratio gradually increases as the spiral diameter increases. When the spiral diameter is 240 mm, the Cu recovery is relatively high, but the enrichment ratio is relatively low, indicating that more SiO_2 is entrained into the concentrate. As the spiral diameter continues to increase, the proportion of SiO_2 entering the concentrate side decreases and the enrichment ratio increases. However, the outer-side enrichment ability and stable recovery effect of Cu particles gradually weaken. Considering both recovery and enrichment ratio, the separation performance is relatively better when the spiral diameter is 260 mm, with a Cu recovery of 58.47% and an enrichment ratio of 12.15.

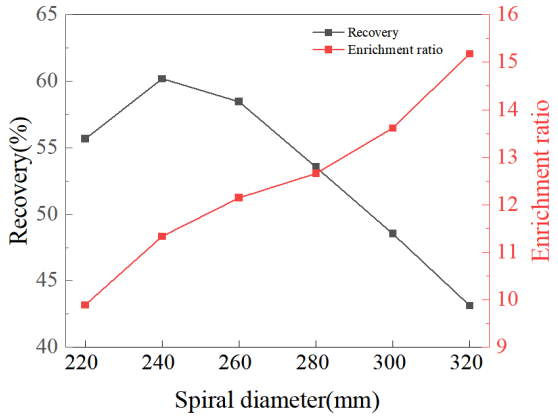

Figure 13. Influence of spiral diameter on the recovery and enrichment ratio of heavy particles

4.4.2. Influence of Pitch on Separation

To analyze the influence of pitch on separation performance, the pitch was set to 40, 50, 60, 70 and 80 mm when the spiral diameter was 260 mm. Pitch mainly affects the axial transport capacity of the slurry along the spiral channel and the residence time of particles in the enrichment section. Under different pitch conditions, the difference in radial velocity in the enrichment section is relatively small, and the change in lateral particle migration capacity is not obvious. As the pitch increases, the axial velocity increases overall, the streamwise transport of the slurry is accelerated, and the residence time of particles in the enrichment section is shortened, which is unfavorable for the sufficient stratification of light and heavy particles. As shown in Figure 14, the recirculation vortex intensity in the secondary sand-splitting section generally increases with increasing pitch. After the pitch increases, the mainstream flow rate entering the secondary sand-splitting section becomes larger, and the recirculation and shear effects behind the abrupt expansion are strengthened. As a result, SiO_2 particles are more likely to detach from the outer particle bed and be entrained away. However, when the pitch is too large, the residence time of particles in the enrichment section is shortened, resulting in insufficient outward enrichment of Cu particles. Meanwhile, stronger recirculation disturbance may also affect the stability of enriched Cu particles.

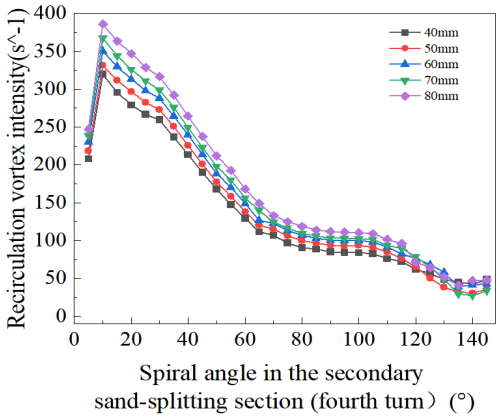

Figure 14. Influence of pitch on recirculation vortex intensity

As shown in Figure 15, the Cu recovery first increases and then decreases with the change in pitch, whereas the enrichment ratio continues to increase as the pitch increases. When the pitch is relatively small, the recirculation effect in the secondary sand-splitting section is weak, resulting in insufficient stripping and entrainment of SiO_2 particles. Consequently, more gangue particles are entrained into the concentrate, leading to a relatively low enrichment ratio. When the pitch is relatively large, although the enrichment ratio increases, the Cu recovery decreases significantly. Considering both recovery and enrichment ratio, the separation performance is relatively better when the pitch is 50 mm, with a Cu recovery of 61.24% and an enrichment ratio of 11.86.

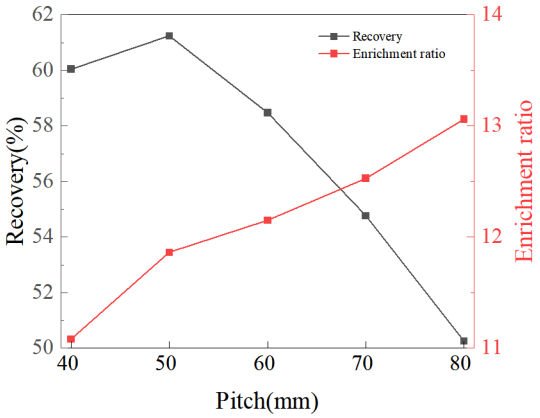

Figure 15. Influence of pitch on the recovery and enrichment ratio of heavy particles

5. Conclusions

(1) The enrichment section can form a stable radial pressure gradient and a relatively high tangential-velocity region. The slurry forms a stable rotational flow in the spiral channel. Under the action of centrifugal force, high-density Cu particles gradually migrate toward the outer enrichment wall and form an enriched bed in the outer bottom region, providing fundamental conditions for the subsequent re-separation in the secondary sand-splitting section.

(2) Owing to the influence of cross-sectional abrupt expansion, the secondary sand-splitting section forms a recirculation vortex that evolves from a counterclockwise single vortex, to double-vortex coexistence, and finally to a clockwise single vortex that gradually decays and disappears. The recirculation vortex intensity first increases and then decreases along the flow path. In this section, the upward jet in the front part strips light particles from the surface layer of the particle bed, and the reverse radial velocity in the rear part laterally entrains the light particles toward the gangue-rich layer, thereby forming a staged separation mechanism of “surface stripping–lateral entrainment” and realizing the selective separation of light and heavy particles.

(3) The particle volume fraction contours show that Cu particles gradually concentrate toward the outer enrichment wall with increasing spiral angle in the enrichment section. After entering the secondary sand-splitting section, Cu particles are still mainly distributed in the outer bottom boss region. SiO_2 particles gradually migrate from the outer particle bed toward the newly formed cavity, the middle-to-upper region and the tailings channel in the secondary sand-splitting section, while the enrichment degree near the outer boss decreases. This indicates that the secondary sand-splitting section can weaken the entrainment of SiO_2 on the concentrate side.

(4) When the spiral diameter is 260 mm and the pitch is 50 mm, the Cu recovery reaches 61.24% and the enrichment ratio is 11.86. Under this condition, the enhanced-gravity spiral trapezoidal pipe exhibits better separation performance for light and heavy particles.

References

[1] Kim, T. Y., Gould, T., Bennet, S., et al. (2021). The role of critical minerals in clean energy transitions (pp. 70–71). International Energy Agency.

[2] Jena, S. S., Tripathy, S. K., Mandre, N. R., et al. (2022). Sustainable use of copper resources: Beneficiation of low-grade copper ores. Minerals, 12(5), 545. https://doi.org/10.3390/min12050545

[3] Feng, Q., Yang, W., Wen, S., et al. (2022). Flotation of copper oxide minerals: A review. International Journal of Mining Science and Technology, 32(6), 1351–1364. https://doi.org/10.1016/j.ijmst.2022.09.008

[4] Ndoro, T. O., & Witika, L. K. (n.d.). A review of the flotation of copper minerals.

[5] Yu, Y., Ma, L., Cao, M., et al. (2017). Slime coatings in froth flotation: A review. Minerals Engineering, 114, 26–36. https://doi.org/10.1016/j.mineng.2017.09.012

[6] (n.d.). Correlation between flotation and rheology of fine particle suspensions.

[7] Chen, X., & Peng, Y. (2018). Managing clay minerals in froth flotation—A critical review. Mineral Processing and Extractive Metallurgy Review, 39(5), 289–307. https://doi.org/10.1080/08827508.2018.1453448

[8] Nzeh, N. S., Popoola, P., Okanigbe, D., et al. (2023). Physical beneficiation of heavy minerals–Part 1: A state of the art literature review on gravity concentration techniques. Heliyon, 9(8). https://doi.org/10.1016/j.heliyon.2023.e18521

[9] Richards, R. G., MacHunter, D. M., Gates, P. J., et al. (2000). Gravity separation of ultra-fine (− 0.1 mm) minerals using spiral separators. Minerals Engineering, 13(1), 65–77. https://doi.org/10.1016/S0892-6875(99)00148-9

[10] Das, A., & Sarkar, B. (2018). Advanced gravity concentration of fine particles: A review. Mineral Processing and Extractive Metallurgy Review, 39(6), 359–394. https://doi.org/10.1080/08827508.2018.1463556

[11] Song, K. W., & Wang, L. B. (2008). Relationship between heat transfer intensity and absolute vorticity flux intensity in flat tube bank fin channels with vortex generators. Progress in Computational Fluid Dynamics, 8(7–8), 496–502. https://doi.org/10.1504/PCFD.2008.018618

[12] Sheen, H. J., Chen, W. J., Jeng, S. Y., et al. (1996). Correlation of swirl number for a radial-type swirl generator. Experimental Thermal and Fluid Science, 12(4), 444–451. https://doi.org/10.1016/0894-1777(95)00142-9